Bragg–Fresnel optics for hard x-ray microscopy: Development of fabrication process and x-ray characterization at the Advanced Photon Source

Youli Li,[a] Gerard C. L. Wong, and Cyrus R. Safinya
Materials Research Laboratory, Materials Department and Physics Department, University of California, Santa Barbara, California 93106

Ernie Caine and Evelyn L. Hu
National Nanofabrication Users Network (NNUN), Electrical and Computer Engineering Department, University of California, Santa Barbara, California 93106

Dean Haeffner, Patricia Fernandez, and Wenbing Yun
Advanced Photon Source, Argonne National Laboratory, Argonne, Illinois 60439

(Received 27 March 1998; accepted for publication 27 May 1998)

Results are presented on development of processes for fabricating linear and circular Bragg–Fresnel lenses (BFLs) on Si and III–V compound material substrates, and on x-ray characterization of linear BFLs at the Advanced Photon Source (APS). Processes were developed for fabricating long (zone length >5 mm) linear BFLs on Si with enhanced capability for focusing high-energy x rays. By stitching together 20 sequentially exposed 400-μm-long linear BFLs, we were able to fabricate 8-mm-long linear BFLs with 0.5-μm finest zone width. BFLs were also fabricated on III–V compound semiconductor substrates GaAs and InP, with improved process control due to the substantially reduced zone thickness required (~50% less than Si). Reduction of the zone aspect ratio (thickness/width) lessens the demand on the process technology, and may lead to higher lens resolution and pattern transfer accuracy. A process was explored to fabricate BFLs on a GaAs/AlGaAs heterostructure incorporating a built-in ''etch stop'' layer to ensure uniform zone thickness. Experimental characterization of the focusing properties of a field-stitched 8-mm-long linear BFL on Si (zone aperture=150 μm) was conducted at APS undulator beamline 1-ID-C using 10-keV x rays. Based on measured focal plane intensity distribution, the focus was estimated to be 1.2 μm, comparable to the geometrically demagnified source size of ~1 μm. Lens efficiency was estimated to be ~30%. Work is underway to incorporate the BFL-microprobe in x-ray microdiffraction and fluorescence microscopy experiments to study spatially confined complex materials. © *1998 American Institute of Physics.* [S0034-6748(98)03508-4]

I. INTRODUCTION

The advent of high-brilliance third-generation synchrotron sources has made possible the effective utilization of diffractive focusing optics, such as Bragg–Fresnel optics, in microprobe-based x-ray diffraction and microscopy experiments. Bragg–Fresnel lenses (BFLs), which are comprised of etched Fresnel zones with a defined thickness for optimal phase focusing on the surface of a single-crystal substrate,[1] are hard x-ray focusing optics with a unique advantage at high x-ray energies (>20 keV) due to the energy-independent focusing capability.[2] To date, a number of experiments,[3–6] mostly conducted at European synchrotron facilities, have demonstrated the effectiveness of BFLs in a broad range of x-ray microdiffraction and direct imaging experiments at submicron spatial resolution with x-ray energies up to above 100 keV. While more applications exploiting the capabilities of BFLs are being explored, it is important to continue optimizing the design, fabrication, and characterization of these optical elements in order to reach a higher level of resolution and performance. In this article we present results of developing fabrication processes and x-ray characterization methods for Bragg–Fresnel optics on Si and III–V compound semiconductor substrates. We report progress in three specific areas: (a) development of field-stitching techniques for fabricating linear Si BFLs with zone lengths on the order of several millimeters and longer, which are particularly well suited for focusing high-energy x rays; (b) development of fabrication processes for making BFLs on III–V compound semiconductor substrates GaAs, InP, and on GaAs-based heterostructures, which require a substantially smaller zone thickness (~50% less than Si) with possible gains in process control and lens quality; and (c) experiments to characterize the focusing capabilities of long linear BFLs on Si at the Advanced Photon Source (APS). Detailed descriptions of the experimental setup and the results of analyzing the focused beam profile are presented.

II. OPTICS FABRICATION

A. BFLs on Si

The BFLs were fabricated using a process consisting of two main steps: electron-beam lithography for pattern definition and reactive ion etching (RIE) for pattern transfer. A

[a]Electronic mail: youli@mrl.ucsb.edu

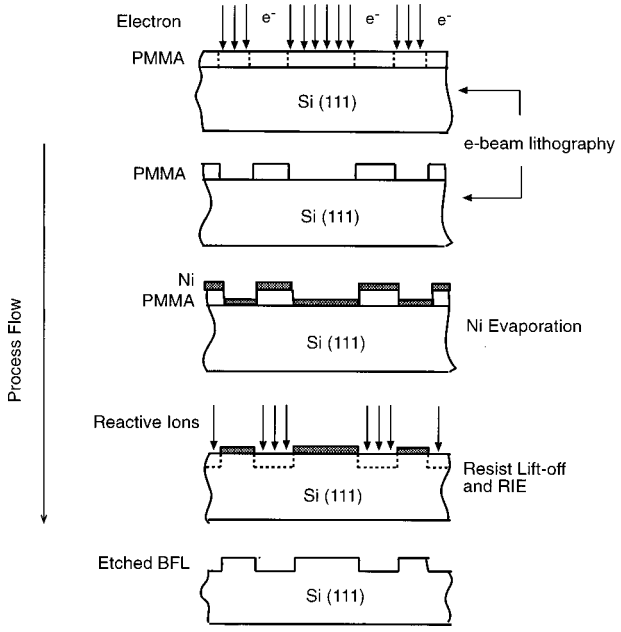

FIG. 1. Process flow chart for fabricating Bragg–Fresnel lenses (BFLs) using e-beam lithography and reactive ion etching. This process was used to fabricate BFLs on III–V compound substrates as well as on Si.

process flow chart illustrating these steps is shown in Fig. 1. Pattern definition on (111)-oriented substrates was achieved using an IBM vector scan e-beam writer, with a 409.6 μm $\times$409.6 μm linearized field defined with a 0.025 μm e-beam. The system allowed us to achieve 0.5 μm finest zone widths consistently. The etch mask was formed by Ni metallization using an e-beam or filament evaporator. Up to 1000 Å thickness of Ni was used depending on zone thickness requirements. A high–low molecular weight double PMMA resist layer (not shown in Fig. 1) was used to facilitate resist lift-off after metallization.[7] The samples were then put into a MRC-51 parallel-plate RIE chamber for transferring the zone pattern into the substrates. A chlorine (Cl_2)-based gas chemistry was used for the Si dry-etching system, with a typical etch rate of 0.1 μm/min. Where applicable, the etched-zone depth was monitored using in-process He–Ne laser interferometry and confirmed by postprocess zone profile measurements using a Sloan Technology DekTak Profilometer and/or scanning electron microscopes (SEM). Si linear BFLs fabricated on (111) substrates require a zone thickness (depth) of 1.26 μm, whereas for circular BFLs the zone thickness depends on the reflection used [3.78 μm for (333) reflection]. The integrity of the etch mask during the etching process is of crucial importance for the deeper circular lenses in order to reach the required zone depth, and nonuniformity in zone depths were generally exacerbated in the high-aspect-ratio outer zones.

Due to the intrinsic property that the required zone thickness in BFLs is independent of x-ray energy, they can be used effectively in a broad x-ray energy range. Of special interest to us is using linear BFLs for microfocusing x rays in the energy range of 20–100 keV, at which other types of microfocusing optics (e.g., transmission zone plates, Kirkpatrick–Baez (K–B) mirrors, and capillary optics) become less effective. However, in the vertical focusing geometry, which is commonly used for linear BFLs, the apparent horizontal aperture of the BFL decreases with increasing x-ray energy as a result of the decreasing Bragg angle. To compensate, it is necessary to increase the length of the BFL accordingly. Long linear BFLs are useful also as two-dimensional focusing optics, with zones bent to produce geometric focusing of the x rays horizontally.[8] With these considerations in mind we fabricated millimeter-long linear BFLs on silicon substrates by stitching together multiple short linear BFLs written within one e-beam scanning field as described earlier. The process is demanding in terms of pattern-stitching accuracy, for any misalignment will directly cause beam broadening when the BFL is used for focusing. Through the use of substrate plane calibration marks, we were able to stitch together 20 one-field BFLs to form a single linear BFL with 8-mm-long zones, 0.15-mm lens aperture, and 0.5 μm outermost zone width. The 8 mm length of the BFL was chosen as an initial test of the process; in principle, the process can be used to make much longer BFLs. Images of the 8-mm-long BFL by optical microscopy and SEM revealed smoothly stitched patterns forming a continuous device, with small lateral displacement of zones evident only upon close examination of the stitching point under high magnification. Due to the high-aspect ratio of the BFL (length/width $>$50), it is not possible to show the entire BFL in one image. In Fig. 2(a) we present a SEM image taken at one end of the 8-mm-long zones, showing about 50% of the width (half the zones) and about 1% of the length of the BFL. The image confirmed a high pattern transfer accuracy with well-defined zone profiles. In Fig. 2(b), we show a close-up plan view of the outermost zone (zone width=0.5 μm) at the stitching point, which is at the center of the image. Based on SEM images taken at various stitching points, we estimated that the average stitching displacement error is roughly 1/5 of the finest zone width, i.e., $\sim$0.1 μm, which is well below the diffraction-limited resolution of the lens. The effect of focus broadening due to this small alignment error is, therefore, practically undetectable with the current lenses. However, the stitching error may eventually become a limiting factor in determining the length of the stitched BFL, as well as the finest zone width which can be achieved. By using state-of-the-art lithography tools, it should be possible to fabricate linear BFLs with 1–2 cm zone length and 0.1–0.2 μm finest zone width.

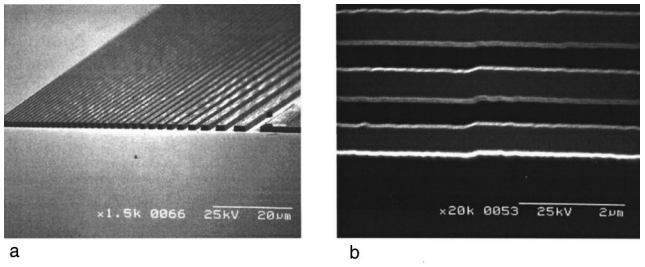

FIG. 2. SEM images of an 8-mm-long linear BFL on Si. (a) At one end of the BFL showing half of the zones. The white speckles on the zone surface are residual Ni from the etch mask, which is removed at the end of processing. (b) Outer zones (zone width=0.5 μm) at one of the stitching points showing dislocation of zones caused by stitching error, which is $\sim$0.1 μm.

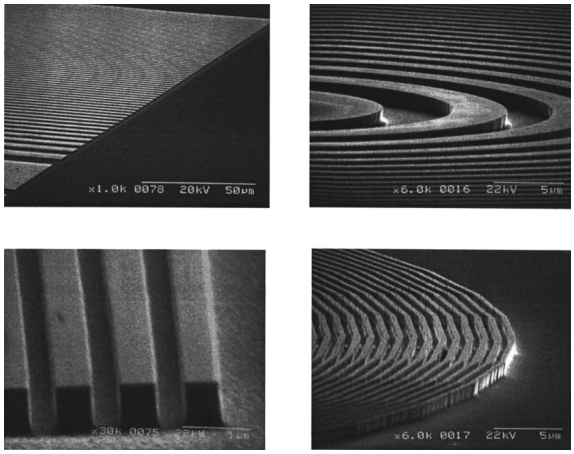

FIG. 3. SEM images of linear and circular BFLs on GaAs substrates. Circular patterns were constructed using sixty-four-sided polygons. Both BFLs have a focal length of 96 cm at 8 keV and outermost zone width of 0.5 μm.

B. BFLs on III–V compound semiconductor substrates and heterostructures

As a result of the nonuniform line spacings in the BFL, the zone aspect ratio (depth/width) varies generally by more than an order of magnitude from the center to the edge of a BFL. At the outer region of the BFL, where the zone aspect ratio is high (>1), the etch rate is reduced due to the ''microloading effect,''[7] which arises from local depletion of the reactive ion species and difficulty of removing ''reacted'' species from the narrow deep zones. This leads to shallower zone depths at the edge of the BFL than in the center, resulting in lower lens efficiency and focus broadening. The problem can be mitigated by making BFLs on III–V compound substrates, which require substantially smaller zone thickness compared to Si. Using a similar process flow designed for Si BFLs, we fabricated linear and circular BFLs on GaAs and InP substrates, with zone thicknesses of 0.53 and 0.57 μm, respectively, for linear (111) lenses. For GaAs substrates, chlorine-based gas chemistry ($BCl_3/Cl_2/SiCl_4$) was used, whereas for InP methane-based chemistry ($CH_4/H_2/Ar$) was used. SEM images of linear and circular BFLs on GaAs are shown in Fig. 3.

One unique advantage of using III–V compound materials for making BFLs is the availability of a wide variety of heterostructures, which allow novel lens designs to be explored. We have tested a process for fabricating BFLs on epitaxially grown GaAs/AlAs/AlGaAs heterostructures, which incorporate a built-in ''etch stop'' layer, as depicted schematically in Fig. 4(a), in order to eliminate nonuniformity of zone depths caused by the ''microloading effect.'' The molecular beam epitaxy (MBE)-grown heterostructure has a 0.53 μm GaAs top layer, the exact thickness of zones for such a linear BFL, with an underlying AlAs/AlGaAs layer as the ''etch stop.'' Heterostructure BFLs were etched using Cl_2/O_2 gas chemistry. During the etching process, the top GaAs layer is first etched through in the central region of the BFL due to the higher etch rate associated with the larger zone widths. This exposes the AlAs/AlGaAs layer, which reacts with O_2 to form nonvolatile and etch-resistant aluminum oxides to effectively stop etching in the central area.

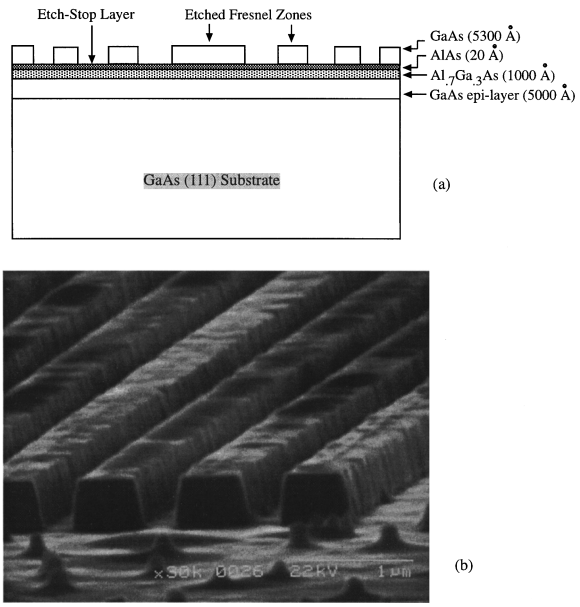

FIG. 4. A linear BFL fabricated on a GaAs heterostructure incorporating a natural ''etch stop'' layer. (a) Schematic cross-sectional view of the MBE-grown heterostructure, (b) SEM image of the heterostructure linear BFL with 0.5 μm finest zone width.

Etching continues in the outer region of the BFL, which has a lower etch rate due to microloading, until the AlAs/AlGaAs layer is reached. This process thus ensures essentially uniform zone depths in the entire BFL (there is some etching occurring in the AlAs/AlGaAs layer, however, the etch rate is substantially reduced). Figure 4(b) shows a SEM image of the outer zones of a GaAs heterostructure BFL. In-process monitoring by laser interferometry confirmed that etching indeed stopped within the AlAs/AlGaAs layer. The etched surface, however, shows some roughness, which likely resulted from differential etch rates caused by local defects in the epitaxial film. Although the extent of detrimental effects of surface roughness on BFLs has yet to be quantified, further MBE growth experimentation may eliminate this problem.

III. X-RAY CHARACTERIZATION OF LINEAR BFLS AT APS

A. Experimental setup

X-ray characterization of linear BFLs was conducted at beamline 1-ID-C at the Advanced Photon Source using 10 keV x rays. The beamline was designed to be a high-energy x-ray optics characterization station with an APS undulator A insertion device and a liquid-nitrogen-cooled Si (311) double-crystal monochromator. The experimental setup for BFL characterization is shown schematically in Fig. 5. Incident x rays coming from the upstream monochromator were defined by a pair of slits (not shown in Fig. 5) located approximately 20 cm upstream of the BFL to match the active area of the BFL. The beam position was calibrated using an x-ray phosphor screen mounted on top of the BFL, and marked on a television monitor connected to a video microscope. This allowed the test BFL to be easily positioned into the path of the x-ray beam using an $x-y-z$ translation stage.

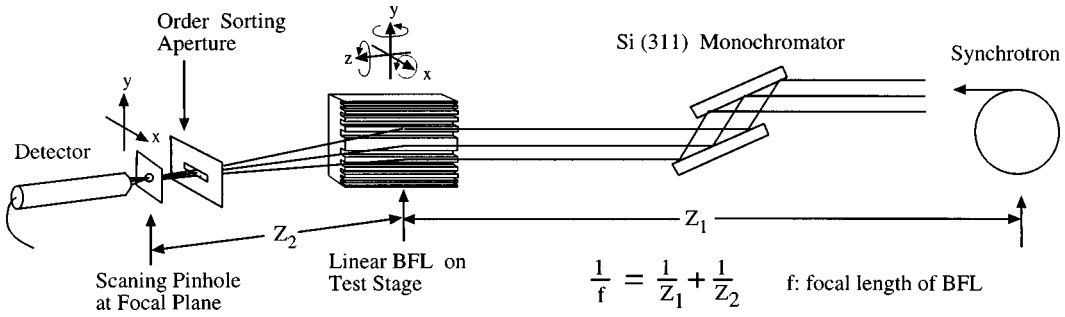

FIG. 5. Experimental setup for characterizing BFLs at beamline 1-ID-C at the Advanced Photon Source (APS). Depiction of upstream optical components on the beamline before the BFL has been greatly simplified.

The BFL was set up with the length of the zones parallel to the incident beam, focusing x rays vertically to take advantage of the higher vertical spatial coherence in the synchrotron radiation. The BFL was set at the desired Si(111) reflection. For the initial characterization of the focused beam, the order-sorting aperture (OSA), which is used to reduce the diffuse background produced by the out-of-focus higher-order foci, was set wide open. The two-dimensional (2D) focal plane intensity distribution (beam profile) was measured using a 10 μm$\times$10 μm pinhole (formed by two pairs of crossed fixed slits) mounted on an $X-Y$ scanning stage. X-ray intensities were recorded using a NaI scintillation detector. With the addition of an energy-dispersive detector, the setup can be readily converted into a hard x-ray scanning fluorescence microscope.

The focusing data presented here were obtained from an 8-mm-long field-stitched Si linear BFL described earlier. The BFL has a focal length of 60.5 cm at 10 keV, an outermost zone width of 0.5 μm, and an aperture size of 150 μm. The vertical source size of the synchrotron at full width at half maxima (FWHM) is approximately 100 μm. At a source- (center of undulator) to-BFL distance of 60 m, the expected focal spot size based on source demagnification is 0.605/60$\times$100 μm $\approx$1.0 μm, which is larger than the diffraction-limited resolution of the lens ($\sim$0.6 μm). Therefore, we expected the focus to be limited by source demagnification rather than lens resolution in this case.

B. Analysis of beam profile data

The focal plane beam profile collected using the setup described above is shown in Fig. 6. The central peak, which corresponds to the first-order focus of the BFL, is riding on a broad bump, which arises mainly from defocused higher-order foci and the unfocused component of the beam (zeroth order). The background can be reduced substantially by using an OSA and a small central beam stop when the BFL is used in microdiffraction and microscopy experiments.[9] In the following, we describe how focal spot size, lens efficiency, and flux density gain were determined from these data. The analysis was performed on a vertical trace of the focusing data through the center of the measured 2D beam profile.

1. Focal spot size

The FWHM of the central peak in the raw data is 11.5 μm, which resulted from convolution of the focused beam with the aperture function of the 10 μm pinhole. A deconvolution process was used to obtain an estimate of the true focal spot size. First, the broad background was fitted to a Gaussian peak and subtracted from the data. An ''Airy disk'' pattern,[9] which approximates the focal plane intensity distribution of a Fresnel zone plate, was convolved with a 10 μm pinhole function to produce the intensity profile to be compared to the measured data. The functional form used to describe the focal plane intensity distribution is $I_0[2J_1(v)/v]^2$, where I_0 is a scaling constant, $v=2\pi(z-z_0)/z_w$, with z being the vertical translation, z_0 the peak position (determined directly from data and not affected by convolution), and z_w the ONLY fitting parameter that controls the width of the focal spot. Iterative corrections were made to z_w to minimize the difference between the width of the resultant peak and the measured peak width. Using a 10 μm sampling pinhole, we obtained a deconvoluted focal spot size (FWHM) of 1.2 μm, compared to the expected focus of 1.0 μm based on source demagnification (see the previous section). Figure 7 shows the comparison between the measured (with the background subtracted) and the fitted data points. There is, however, some uncertainty as to the effective size of the pinhole, which arises due to the finite thickness of the slit edge. Based on optical microscopy and x-ray transmission measurements, we have established a lower bound of 9 μm for the effective pinhole size, which led to an upper bound of 3 μm for the focal spot size. Direct measurement of the focal spot size will be made in future experiments by using the focused beam to image Au grid patterns with submicron linewidths.

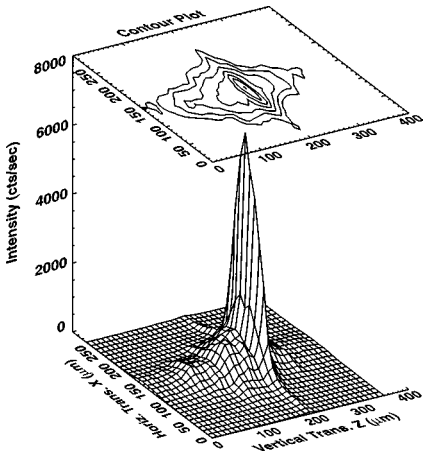

FIG. 6. X-ray beam profile at the focal plane of the linear BFL measured with a 10 μm scanning pinhole.

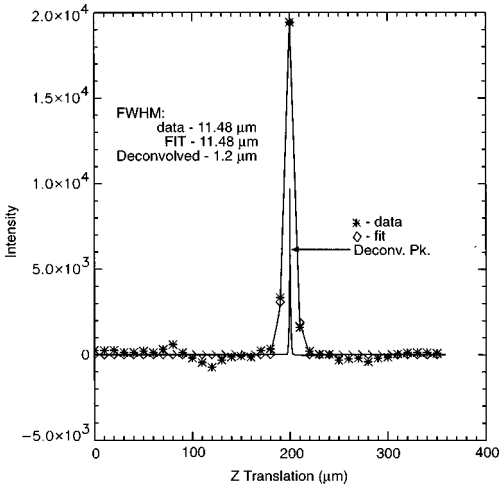

FIG. 7. Comparison of measured intensity distribution and that fitted by the deconvolution process. The deconvolved peak shown in the center has a FWHM of 1.2 μm, which is the focal spot size of the BFL.

2. Lens efficiency

BFLs are pure phase lenses, which modify only the distribution but not the total photon flux in the reflected beam. It is, therefore, possible to estimate the first-order focusing efficiency of the BFL by calculating the ratio of intensity in the focus (no deconvolution needed) to the integrated intensity in the entire measured area (this excludes the effect of substrate reflectivity). Extraneous background was determined by averaging pixel intensities at one corner of the 2D beam profile and was subtracted from the data. We obtained an efficiency of 30% based on the one-dimensional focusing data extracted from the center of the 2D beam profile (the central peak point was taken as the focus). This efficiency is lower than the theoretical efficiency of ~40% for a BFL with a rectangular zone profile,[9] which may be attributed to the inherent uncertainty in the method used for deriving the experimental efficiency, as well as the partial incoherence of the incident beam which causes focus broadening and reduces lens efficiency.

3. Flux–density gain

Flux–density gain (flux/area) due to focusing was roughly estimated by dividing the size of the incident beam (150 μm) by the deconvolved focal spot size (1.2 μm), and multiplied by the lens efficiency (30%). This gave a flux–density gain of ~38 for the linear BFL we characterized, compared to a theoretical gain of 100 if diffraction-limited focus (0.6 μm) was obtained with full first-order efficiency (40%). A higher degree of beam compression is achievable using BFLs with smaller finest zone widths and a larger source demagnification ratio. A fourfold increase of flux–density gain can be realized with a twofold reduction of finest zone widths, due to the fact that at constant focal length the diffraction-limited resolution decreases and the lens aperture increases linearly with the finest zone width. We are currently working on making BFLs with 0.25 μm linewidths, with a theoretical flux–density gain >400 for one-dimensional focusing. Two-dimensional focusing, which can increase the flux–density gain substantially, can be achieved with two linear BFLs arranged in K–B geometry[10,11] or by geometric focusing through bending of the linear BFL.[8] Flux–density gains $>10^3$ are possible with these setups.

IV. DISCUSSION

Development of fabrication processes and x-ray characterization methods for Bragg–Fresnel lenses were presented. BFLs were fabricated on Si, GaAs, and InP substrates. A process to fabricate BFLs on GaAs-based heterostructures with a built-in ''etch-stop'' layer was explored. Experiments conducted at the Advanced Photon Source for characterizing the x-ray focusing properties of BFLs were described. Future developments will concentrate on fabricating higher-resolution lenses (i.e., smaller linewidths) and on utilizing BFLs in hard x-ray microdiffraction and microscopy experiments.

ACKNOWLEDGMENTS

The authors thank Sunil K. Sinha for help in arranging beamtime at the APS. This work is support by the National Science Foundation under Award No. DMR-9625977 and DNR Grant No. N00014-93-1-0269. The Materials Research Laboratory at U.C. Santa Barbara is supported by NSF-DMR-9632716. Use of the Advanced Photon Source was supported by the U.S. Department of Energy, Basic Energy Sciences, Office of Energy Research, under Contract No. W-31-109-Eng-38. The characterization was carried out at the 1-ID-C beamline, which is operated by the synchrotron Radiation Instrumentation Collaborative Access Team (SRI-CAT).

[1] V. V. Aristov, Y. A. Basov, and A. A. Snigirev, Rev. Sci. Instrum. **60**, 1517 (1989).
[2] V. V. Aristov, Y. A. Basov, A. A. Snigirev, V. A. Yunkin, T. Ishikawa, and S. Kikuta, Nucl. Instrum. Methods Phys. Res. A **308**, 413 (1991).
[3] A. Snigirev, I. Snigireva, P. Bosecke, S. Lequien, and I. Schelokov, Opt. Commun. **135**, 378 (1997).
[4] Y. Hartman, V. Kohn, S. Kuznetsov, A. Snigirev, and I. Snigireva, Nuovo Cimento B **19**, 571 (1997).
[5] A. Firsov, A. Svintsov, A. Firsova, P. Chevallier, and P. Populus, Nucl. Instrum. Methods Phys. Res. A **399**, 152 (1997).
[6] A. Erko, Y. Agafonov, L. A. Panchenko, A. Yakshin, P. Chevallier, P. Dhez, and F. Legrand, Opt. Commun. **106**, 146 (1994).
[7] E. J. Caine, S. Shi, E. L. Hu, Y. Li, S. H. J. Idziak, G. Subramanian, and C. R. Safinya, Microelectron. Eng. **35**, 289 (1997).
[8] Y. Hartman, A. K. Freund, I. Snigireva, A. Souvorov, and A. Snigirev, Nucl. Instrum. Methods Phys. Res. A **385**, 371 (1997).
[9] A. G. Michette, *Optical Systems for Soft X Rays* (Plenum, New York, 1986).
[10] U. Bonse, C. Riekel, and A. A. Snigirev, Rev. Sci. Instrum. **63**, 622 (1992).
[11] P. Dhez, A. Erko, E. Khzmalian, B. Vidal, and V. Zinenko, Appl. Opt. **31**, 6662 (1992).